Multi-Dimensional Continuous Metric for Mesh Adaptation

Frédéric Alauzet[1], Adrien Loseille[1], Alain Dervieux[2], and Pascal Frey[3]

[1] INRIA-Gamma, Domaine de Voluceau, BP 105, 78153 Le Chesnay cedex, France
Frederic.Alauzet@inria.fr and Adrien.Loseille@inria.fr
[2] INRIA-Tropics, BP 93, 06902 Sophia-Antipolis, France
Alain.Dervieux@inria.fr
[3] UMPC/Lab. J-L Lions, BP 187, 75252 Paris Cedex 05, France
frey@ann.jussieu.fr

Summary. Mesh adaptation is considered here as the research of an optimum that minimizes the $\mathcal{P}_1$ interpolation error of a function u of $\mathbb{R}^n$ given a number of vertices. A continuous modeling is described by considering classes of equivalence between meshes which are analytically represented by a metric tensor field. Continuous metrics are exhibited for $\mathbf{L}^p$ error model and mesh order of convergence are analyzed. Numerical examples are provided in two and three dimensions.

Key words: Continuous metric, metric tensor, mesh adaptation, anisotropy, interpolation error, order of convergence

1 Introduction

Nowadays, in the context of numerical simulations based on finite elements or finite volumes methods, unstructured mesh adaptation has largely proved its efficiency for improving the accuracy of the numerical solution as well as for capturing the behavior of physical phenomena. In principle, this technique allows (i) to substantially reduce the number of degrees of freedom, thus impacting favorably the cpu time and (ii) to automatically capture the anisotropy of the physical phenomena. However, such efficiency is usually observed from the practical point of view only, as a thorough theoretical analysis is really tedious to carry out on unstructured meshes. Indeed, there is no simple Hilbert space structure for the type of non-isotopological meshes that are required for a variational study. To overcome this difficulty, we represent meshes with continuous functions describing them. To this end, the concept of continuous metric, introduced by Dervieux et al. [19, 7], is used to replace the notion of a mesh in a variational analysis. A continuous metric is simply a continuous function associating a metric tensor to each vertex of the domain.

Over the last few years, numerous papers have been published concerning mesh adaptation in numerical simulations. It points out that isotropic mesh adaptation has been already well addressed in two and three dimensions, see for instance [12, 2, 18, 22, 24, 25, 21, 27]. Regarding anisotropic mesh adaptation, numerous works using (or implicitly using) the concept of metric in order to equally distribute the interpolation error have been published in two dimensions [1, 3, 4, 10, 9, 17]. However, only a few of them have dealt with the three-dimensional case [13, 16, 20, 28, 23].

Recently, some papers have proposed a new approach to define an optimal metric in two dimensions for minimizing the interpolation error in norm $\mathbf{L}^p$ in order to generate anisotropic adapted meshes [26, 6, 5]. Formally speaking, let u be an analytic solution defined on a bounded domain Ω and let N denotes the desired number of vertices for the mesh, the aims is to to create the "best" mesh $\mathcal{H}$, i.e., the best continuous metric $\mathcal{M}$, to minimize the interpolation error $\|u - \Pi_h u\|_p$ in $\mathbf{L}^p$ norm, $\Pi_h u$ being the linear interpolate of u on $\mathcal{H}$. To this end, a model of the interpolation error $e_{\mathcal{M}}$ is required. Once $e_{\mathcal{M}}$ has been properly defined, a calculus of variation is performed on the domain Ω. Mathematically, we need to solve the following minimization problem:

$$\text{find } \mathcal{E}(\mathcal{M}) \text{ such that } \min_{\mathcal{M}} \int_{\Omega} |e_{\mathcal{M}}(\mathbf{x})|^p \, \mathrm{d}\mathbf{x}. \tag{1}$$

The aim of this paper is to extend the results presented in two dimensions in [6] in any dimension. Firstly, we indicate how we get our local error model $e_{\mathcal{M}}$ based on a bound of the interpolation error. We also demonstrate that the optimal directions of the desired metric coincide with the directions of the Hessian of the solution. Secondly, to extend the result in dimension n, we propose a definition of anisotropic quotients. A coordinate transformation is performed with these quotients to simplify the resolution of Problem (1) by a calculus of variation. Finally, we analyze the order of convergence of the error with respect to the obtained optimal metric.

Analytical examples in two and three dimensions are given to illustrate the impact of the continuous metric throughout a mesh adaptation process.

2 Metric Notions

The notion of length in a metric space is closely related to the notion of metric and subsequently to the definition of the scalar product in the vector space. When this metric is continuously defined over the whole domain, it is called a *continuous metric*. In the following, the natural scalar dot product of $\mathbb{R}^n$ is denoted by $\langle\ ,\ \rangle$.

Metric Definition

A *metric tensor* (or, more simply, a *metric*) $\mathcal{M}$ in $\mathbb{R}^n$ is a $n \times n$ symmetric strictly definite positive matrix; hence $\mathcal{M}$ is always diagonalizable.

From this definition, it follows up that the *scalar product* of two vectors in $\mathbb{R}^n$ is defined with respect to a metric $\mathcal{M}$ as:

$$\langle \mathbf{u}\,,\,\mathbf{v}\rangle_{\mathcal{M}} = \langle \mathbf{u}, \mathcal{M}\mathbf{v}\rangle = {}^t\mathbf{u}\,\mathcal{M}\,\mathbf{v} \in \mathbb{R}\,.$$

Under this notion, the Euclidean *norm* of a vector in $\mathbb{R}^n$ is easily defined as:

$$\|\mathbf{u}\|_{\mathcal{M}} = \sqrt{\langle \mathbf{u}\,,\,\mathbf{u}\rangle_{\mathcal{M}}} = \sqrt{{}^t\mathbf{u}\,\mathcal{M}\,\mathbf{u}}\,,$$

that actually measures the length of vector $\mathbf{u}$ with respect to metric $\mathcal{M}$.

A metric $\mathcal{M}$ could be geometrically represented by its associated unit ball, an ellipsoid, defined as:

$$\mathcal{E}ll_{\mathcal{M}} = \{b\,|\sqrt{{}^t\overrightarrow{ab}\,\mathcal{M}\,\overrightarrow{ab}} = 1\}$$

where a denotes the center of the ellipsoid. The main axes are given by the eigenvectors of matrix $\mathcal{M}$ and the radius along each axis is given by the inverse of the square root of the associated eigenvalues.

In the following sections, the metric unit ball is essentially used to define neighborhoods. We denote by $\mathcal{B}_{\mathcal{M}}(a)$ the unit ball of a in metric $\mathcal{M}$, also defined as:

$$\mathcal{B}_{\mathcal{M}}(a) = \{b \in \mathbb{R}^n \,|\, d_{\mathcal{M}}(a,b) \leq 1\,\}.$$

More details on these notions can be found in [14].

Continuous Metric

Let $\Omega \subset \mathbb{R}^n$ be the computational bounded domain. Defining a continuous metric on Ω is equivalent to define an Euclidean space supplied with a Riemannian metric $(\Omega, \mathcal{M}(.))$, where $\mathcal{M}(.)$ is the continuous metric. In this case, the distance between two points a and b is given by the integral:

$$d_{\mathcal{M}}(a,b) = \int_0^1 \sqrt{{}^t\overrightarrow{ab}\mathcal{M}(\gamma(t))\overrightarrow{ab}}\,\mathrm{d}t, \tag{2}$$

where $\gamma(t) = a + t\,\mathbf{ab}$ is a normal parametrization of the arc ab.

A mesh is called a *unit mesh* with respect to the continuous metric $\mathcal{M}(.)$ if all its edges have a length strictly equal (or very close) to one in the continuous metric $\mathcal{M}(.)$, as given by Relation (2) and if all its elements are (almost) regular.

This notion of a continuous metric is a trick that allows us to forsake the mesh in the analysis. Indeed, a mesh generator governed by a metric tensor field makes use of the distance criterion specified by the continuous metric. Therefore, two different *unit meshes* with respect to this metric can be considered as strictly equivalent. This metric defines a class of equivalence between meshes. In this respect, the mesh becomes an unknown of the problem with respect to a continuous metric.

Notations

In the following, a continuous metric $\mathcal{M}$ defines for any point a of the domain $\Omega \in \mathbb{R}^n$ a matrix $\mathcal{M}(a)$. For sake of simplicity we omit a in our notations, we denote by $\mathcal{M}$ instead of $\mathcal{M}(a)$ the continuous metric. This continuous metric is always diagonalized. We define the following functions as unknowns of our problem:

- let $\mathcal{R}_{\mathcal{M}}$ be the function associating to each point a of the domain $\Omega \in \mathbb{R}^n$ the coordinate transformation matrix of $\mathcal{M}(a)$. $\mathcal{R}_{\mathcal{M}}$ is composed with the eigenvectors $(\mathbf{v}_1, \mathbf{v}_2, .., \mathbf{v}_n)$ of $\mathcal{M}$.
- let be $\lambda_1, \lambda_2, .., \lambda_n$ the n functions associating to each point a of the domain the eigenvalues of $\mathcal{M}(a)$. Or similarly, we could denote by $h_1, h_2, .., h_n$ the local size functions defined by $h_i = \sqrt{1/\lambda_i}$ for $i = 1, ..., n$.

For a unit mesh, an edge parallel to $\mathbf{v}_i$ should be, according to (2), of length equal to $h_i = \sqrt{1/\lambda_i}$, where h_i is the local mesh size in direction $\mathbf{v}_i$.

If the distance in a metric space is defined by a metric, the latter also indicates the vertex density (or distribution) over the domain directly from the local sizes $(h_i)_{i=1..n}$. Indeed, let d be the mesh density, defined as $d = \prod_{i=1}^{n} h_i^{-1}$, then the number of vertices $\mathcal{C}(\mathcal{M})$ of the mesh, or *the mesh complexity*, is given by:

$$C(\mathcal{M}) \;=\; \int_{\mathbf{x}\in\Omega} d(\mathbf{x})\,\mathrm{d}\mathbf{x} \;=\; \int_{\mathbf{x}\in\Omega} \prod_{i=1}^{n} \frac{1}{h_i}(\mathbf{x})\,\mathrm{d}\mathbf{x}.$$

Let u be a C^2 continuous function, we denote its Hessian by $H_u = \left(\dfrac{\partial u}{\partial x_i \partial x_j}\right)_{i,j}$. It can be decomposed as follows:

$$H_u = \mathcal{R}_u\, \Lambda\, \mathcal{R}_u^{-1} = \mathcal{R}_u \mathrm{diag}\left(\frac{\partial^2 u}{\partial {\alpha_i}^2}\right) \mathcal{R}_u^{-1},$$

where $\mathcal{R}_u$ is formed by the eigenvectors of H_u denoted $(\mathbf{u}_1, \mathbf{u}_2, .., \mathbf{u}_n)$. If the diagonal matrix Λ has all non-zero terms, then the matrix $|H_u|$ is a metric tensor defined as:

$$|H_u| = \mathcal{R}_u\, |\Lambda|\, \mathcal{R}_u^{-1} = \mathcal{R}_u \mathrm{diag}\left(\left|\frac{\partial^2 u}{\partial {\alpha_i}^2}\right|\right) \mathcal{R}_u^{-1}\,. \tag{3}$$

3 Local Error Modeling

In this section, the local error $e_{\mathcal{M}}(a)$ in the neighborhood of a vertex a is designed. This error is evaluated in the neighborhood $\mathcal{B}_{\mathcal{M}}(a)$ of a defined by the continuous metric $\mathcal{M}$. We first express this error in terms of the discrete error e_K, the interpolation error in $\mathbf{L}^\infty$ norm on an element K of mesh $\mathcal{H}$ considered as a representative of the continuous metric $\mathcal{M}$. Next, we demonstrate

that this error is maximal when its main directions $(\mathbf{v}_1, \mathbf{v}_2, .., \mathbf{v}_n)$ are aligned with the main directions of the Hessian $(\mathbf{u}_1, \mathbf{u}_2, .., \mathbf{u}_n)$. Then, we obtain the following local error model:

$$e_{\mathcal{M}}(a) = \sum_{i=1}^{n} h_i^2 \left| \frac{\partial^2 u}{\partial {\alpha_i}^2} \right| .$$

3.1 Local Error Definition

Let a be a point of domain Ω and let $\mathcal{B}_{\mathcal{M}}(a) = \{\mathbf{x} \in \Omega \mid d_{\mathcal{M}}(\mathbf{x}, a) \leq 1\}$ denotes its unit ball. The aim is to control the local error $e_{\mathcal{M}}$ in the vicinity of a defined as:

$$e_{\mathcal{M}}(a) = \max_{\mathbf{x} \in \mathcal{B}_{\mathcal{M}}(a)} |u(\mathbf{x}) - \Pi_h u(\mathbf{x})|.$$

Practically, we need a discrete support to be able to compute this error. To follow up on this idea, we consider a mesh $\mathcal{H}$ as a member of the class of equivalence defined by $\mathcal{M}$ and a as a vertex of this mesh. As the mesh is represented by $\mathcal{M}$, the unit ball $\mathcal{B}_{\mathcal{M}}(a)$ is represented on $\mathcal{H}$ by $\mathcal{B}_h(a)$, its ball in the mesh, i.e., the set of all mesh vertices connected to the vertex a. Indeed, $\mathcal{H}$ is a unit mesh for $\mathcal{M}$, then the lengths of all edges ab, $b \in \mathcal{B}_h(a)$ are equal to one with respect to the metric. Consequently, we propose the following model for the local error on the mesh $\mathcal{H}$:

$$e_{\mathcal{M}}(a) = \max_{K \in \mathcal{B}_h(a)} \|u - \Pi_h u\|_{\infty, K} = \max_{K \in \mathcal{B}_h(a)} e_K. \tag{4}$$

Therefore, we need to compute the interpolation error on an element K in $\mathbf{L}^\infty$ norm to model the local error. This will be explained in the next section.

3.2 The Discrete Case

In this section, a geometric error estimation of the interpolation error in $\mathbf{L}^\infty$ norm is presented. This error estimate will be used hereafter to construct our error model. Here, we will focus exclusively on the three-dimensional case.

We consider a tetrahedral unstructured mesh with the following notations:

- $K = [a, b, c, d]$ is a tetrahedron with a diameter not necessary supposed small
- $u : \mathbb{R}^3 \longrightarrow \mathbb{R}$ is a (regular) function representing the solution of our problem
- $\Pi_h u$ is the linear interpolate of u on the element K defined by the parameterization $\Pi_h u = (1 - \lambda - \mu - \nu)u(a) + \lambda u(b) + \mu u(c) + \nu u(d)$, with $0 \leq \lambda + \mu + \nu \leq 1$.

The aim is to bound the error $e = u - \Pi_h u$ on K. To this end, we rely on a Taylor expansion with an integral rest of the function e at a vertex of K (for instance a) with respect to any interior point x in K:

$$(u - \Pi_h u)(a) = (u - \Pi_h u)(x) + \langle \overrightarrow{xa}\,,\, \nabla(u - \Pi_h u)(x)\rangle + \int_0^1 (1-t)\,\langle \overrightarrow{ax}\,,\, H_u(x + t\overrightarrow{xa})\,\overrightarrow{ax}\rangle\, dt\,,$$

where $\nabla u(x)$ and $H_u(x)$ denote the gradient and the Hessian of the variable u at point x, respectively. Actually, as we assume that the maximal error is achieved at the location x (closer to a than to b, c or d), then $\nabla(u - \Pi_h u)(x) = 0$ and as u and $\Pi_h u$ coincide at the vertex a by definition, we get:

$$|e(x)| = |\int_0^1 (1-t)\,\langle \overrightarrow{ax}\,,\, H_u(x + t\overrightarrow{xa})\,\overrightarrow{ax}\rangle\, dt\,|\,.$$

Let a' representing the point corresponding to the intersection of the line ax with the face opposite to a. It exists a real number λ such that $\overrightarrow{ax} = \lambda\overrightarrow{aa'}$. As a is closer to x than to any other vertex of K, $\lambda \leq 3/4$, it yields:

$$\begin{aligned} |e(x)| &= |\int_0^1 (1-t)\,\lambda^2\,\langle \overrightarrow{aa'}\,,\, H_u(a + t\overrightarrow{xa})\,\overrightarrow{aa'}\rangle\, dt\,|\,, \\ &\leq \frac{9}{16}\max_{y\in aa'} |\,\langle \overrightarrow{aa'}\,,\, H_u(y)\,\overrightarrow{aa'}\rangle\,|\;|\int_0^1 (1-t)\,dt\,|\,, \end{aligned}$$

and then:

$$|e(x)| \leq \frac{9}{32}\max_{y\in K} |\,\langle \overrightarrow{aa'}\,,\, H_u(y)\,\overrightarrow{aa'}\rangle\,|\,.$$

At this point, we can introduce the $\mathbf{L}^\infty$ norm of the interpolation error and consider the symmetric definite positive matrix $|H_u|$ (cf. Section 2). The following bound is obtained:

$$\|u - \Pi_h u\|_{\infty,K} \leq \frac{9}{32}\max_{y\in K} \langle \overrightarrow{aa'}\,,\, |H_u(y)|\,\overrightarrow{aa'}\rangle\,.$$

Notice that the previous relationship is not very useful in practice as the bound depends on the extremum x that is not known *a priori*. However, it can be reformulated in a more practical manner as follows:

$$e_K = \|u - \Pi_h u\|_{\infty,K} \leq \frac{9}{32}\max_{y\in K}\max_{\mathbf{v}\subset K} \langle \mathbf{v}\,,\, |H_u(y)|\,\mathbf{v}\,\rangle\,, \tag{5}$$

where $\mathbf{v} \subset K$ means that $\mathbf{v}$ is a vector inside the element K, i.e., there exist two points $m, n \in K$ such that $\mathbf{v} = \overrightarrow{mn}$.

This expression provides a bound in the case where the maximum error is achieved inside the element K. If the maximum error is obtained on the element face, then we obtain:

$$e_K = \|u - \Pi_h u\|_{\infty,K} \leq \frac{2}{9} \max_{y\in[a,b,c]} \max_{\mathbf{v}\subset[a,b,c]} \langle \mathbf{v}\,,\, |H_u(y)|\,\mathbf{v}\,\rangle\,.$$

Similarly, for a maximum value obtained along an element edge, we have:

$$e_K = \|u - \Pi_h u\|_{\infty,K} \leq \frac{1}{8} \max_{y\in ab} \langle \overrightarrow{ab}\,,\, |H_u(y)|\,\overrightarrow{ab}\rangle\,.$$

In conclusion, Relation (5) provides a convenient bound of the interpolation error on an element K.

Remark 1. This proof can be extended to any dimension n using a recurrence relation where the constant is given by:

$$c_n = \lambda^2 |\int_0^1 (1-t)\mathrm{d}t\,| = \frac{1}{2}\left(\frac{n}{n+1}\right)^2.$$

3.3 Optimal Directions

From the previous section, the local error $e_{\mathcal{M}}$ in the neighborhood of a is defined by Relation (4) and for any simplex K of $\mathbb{R}^n$ we have:

$$e_K = c_n \max_{y\in K} \max_{\mathbf{v}\subset K} \langle\, \mathbf{v},\, |H_u(y)|\mathbf{v}\,\rangle \leq \max_{y\in K} \max_{\mathbf{v}\subset K} \langle\, \mathbf{v},\, |H_u(y)|\mathbf{v}\,\rangle. \tag{6}$$

We note that right-hand side of Relation (6) is a second order estimate since $\|\mathbf{v}\|_2$ is smaller than the diameter of element K. In the proposed modeling, we neglect third order terms, which allows us to replace $\max_{y\in K} f(y)$ by $f(a)$ in the neighborhood $\mathcal{B}_{\mathcal{M}}(a)$. The right-hand side of Relation (6) is used to model the interpolation error e_K. In consequence, Equation (4) is written in a more simple form as:

$$e_{\mathcal{M}}(a) = \max_{K\in\mathcal{B}_h(a)} \max_{\mathbf{v}\subset K} \langle\, \mathbf{v},\, |H_u(a)|\mathbf{v}\,\rangle\,.$$

The set of eigen-vectors $(\mathbf{v}_1, \mathbf{v}_2, .., \mathbf{v}_n)$ of $\mathcal{M}$ forms a basis of $\mathbb{R}^n$. Hence, any vector $\mathbf{v}$ inside $\mathcal{B}_h(a) \subset \mathcal{B}_{\mathcal{M}}(a)$ can be written in this basis such as $\mathbf{v} = \sum_{i=1}^n \nu_i \mathbf{v}_i$ which could be also written $\mathbf{v} = \sum_{i=1}^n \mu_i h_i \mathbf{v}_i$ with $\|\boldsymbol{\mu}\|_2 = \sum_{i=1}^n \mu_i^2 \leq 1$. Finally, from Expression (3), we have to compute the expression:

$$e_{\mathcal{M}}(a) = \max_{\|\boldsymbol{\mu}\|_2\leq 1} \sum_{j=1}^n \left(\sum_{i=1}^n \mu_i h_i \langle \mathbf{v}_i, \mathbf{u}_j\rangle\right)^2 \left|\frac{\partial^2 u}{\partial {\alpha_j}^2}\right|. \tag{7}$$

Problem (7) could be written in a matrix form as follows:

$$e_{\mathcal{M}}(a) = \max_{\|X\|_2\leq 1} (HPX)^T |\Lambda| HPX, \tag{8}$$

where

- X is the unknown vector of the μ_i
- H and $|\Lambda|$ are the diagonal matrices $\mathrm{diag}(h_i)$ and $\mathrm{diag}(\left|\frac{\partial^2 u}{\partial {\alpha_i}^2}\right|)$, respectively
- P is the transformation matrix from the eigen-basis of $\mathcal{M}$ to that of $|H_u|$, defined by $P = (P_{ij})_{ij} = (\langle \mathbf{u}_i \,|\mathbf{v}_j\rangle)_{ij}$.

We consider the one to one variable substitution $Y = PX$. As the orthogonal matrix P preserves the norm, Problem (8) is equivalent to the following:

$$e_{\mathcal{M}}(a) = \max_{\|Y\|_2 \leq 1} (HY)^T |\Lambda| HY = \max_{\|\mathbf{y}\|_2 \leq 1} \sum_{i=1}^{n} h_i^2 \, y_i^2 \left| \frac{\partial^2 u}{\partial {\alpha_i}^2} \right|, \tag{9}$$

here, the vector Y has been written as $(y_1, y_2, .., y_n)$. It yields:

$$\max_{\|Y\|_2 \leq 1} (HY)^T |\Lambda| HY \leq \max_{j=1..n} \left(h_j^2 \left| \frac{\partial^2 u}{\partial {\alpha_j}^2} \right| \right) \sum_{i=1}^{n} y_i^2.$$

Therefore, the constraint is active, i.e., the maximum is reached for $\|Y\| = 1$, and we get the following equality:

$$\max_{\|Y\|_2 \leq 1} (HY)^T |\Lambda| HY = \max_{i=1..n} \left(h_i^2 \left| \frac{\partial^2 u}{\partial {\alpha_i}^2} \right| \right) .$$

To find the optimal directions, we differentiate the Lagrangian $\mathcal{L}$ associated with Problem (9). Let λ be the Lagrange multiplier associated with the constraint $\|Y\|^2 = 1$, which is equivalent to the initial constraint. This constraint replaces the initial one as it is differentiable. The optimality condition $\nabla \mathcal{L}(Y, \lambda) = 0$ is equivalent to the system:

$$\begin{cases} \vdots \\ 2y_i \left(h_i^2 \left| \frac{\partial^2 u}{\partial {\alpha_i}^2} \right| - \lambda \right) = 0 \qquad \text{for } i = 1, ..., n\,. \\ \vdots \end{cases}$$

The n solution vectors Y_i, $i = 1, ..., n$ are such that:

$$y_i = 1 \text{ and } y_j = 0 \text{ for } j \neq i \quad \text{and} \quad \lambda = h_i^2 \left| \frac{\partial^2 u}{\partial {\alpha_i}^2} \right|.$$

Going back to the initial problem, the n solution vectors X_i are finally:

$$X_i = P^{-1} Y_i = \mathbf{u}_i \,.$$

The previous demonstration indicates that the optimal directions of the metric are aligned with the main directions of the Hessian. Replacing the value of X_i back in Relation (7), the local error model now becomes:

$$e_{\mathcal{M}}(a) = \sum_{i=1}^{n} h_i^2 \left| \frac{\partial^2 u}{\partial {\alpha_i}^2} \right| . \tag{10}$$

In the remainder of paper, we consider that the optimal direction are those of H_u. However, we still have to compute the optimal sizes.

4 Calculus of Variation

From the previous section, we know that the interpolation error in the neighborhood of the vertex a could be modelled by Relation (10). Now, we are looking for a function $\mathcal{M}$ that minimizes, for a given number N of vertices, the $\mathbf{L}^p$ norm of this error. To this end, we have to solve the following problem:

$$\min_{\mathcal{M}} \mathcal{E}(\mathcal{M}) = \min_{\mathcal{M}} \int_{\Omega} (e_{\mathcal{M}}(\mathbf{x}))^p \, \mathrm{d}\mathbf{x} = \min_{h_i} \int_{\Omega} \left(\sum_{i=1}^{n} h_i^2(\mathbf{x}) \left| \frac{\partial^2 u}{\partial {\alpha_i}^2}(\mathbf{x}) \right| \right)^p \mathrm{d}\mathbf{x}, \tag{11}$$

under the constraint:

$$\mathcal{C}(\mathcal{M}) = \int_{\Omega} \prod_{i=1}^{n} h_i^{-1}(\mathbf{x}) \, \mathrm{d}\mathbf{x} = \int_{\Omega} d(\mathbf{x}) \, \mathrm{d}\mathbf{x} = N. \tag{12}$$

In the following, a formal resolution scheme is proposed. Then we check that the resulting solution is indeed a metric and is also the sole minimum.

4.1 Anisotropic Quotients in Dimension n

We notice that if the local sizes h_i are used as unknowns then Constraint (12) is non linear, however the constraint is linear with respect to the density $d = \prod_{i=1}^{n} h_i^{-1}$. Nevertheless, if d is introduced as an unknown, then one of the h_i will be removed, thus removing a certain symmetry. Moreover, anisotropic ratios r_i, which relate all the sizes i.e., $r_i = f(h_1, h_2, .., h_n)$, may be naturally extracted from the metric. Instead of keeping h_i as variables, we shall use what we call anisotropic quotients. Let us propose a definition of anisotropic quotients in dimension n.

The idea is to define a notion of an anisotropic quotient very similar to the notion of an anisotropic ratio in two dimensions and that can be easily extended to any dimension. Indeed, none clear definition of the anisotropic ratio is known by the authors in three dimensions. Then, this definition will be used to perform a substitution of variables to obtain as unknown the first $n-1$ anisotropic quotients r_i and the density d.

We define the ith anisotropic quotient in dimension n as:

$$r_i = \left(\frac{h_i^n}{\prod_{k=1}^{n} h_k} \right)^{1/n}.$$

The advantage of this definition is to provide a simple geometric interpretation in terms of the ratio of hyper-volumes. In two dimensions, this quotient is simply the square root of the anisotropic ratio.

From the previous definition, the following variable substitution is considered to solve Problem (11)-(12):

$$(h_i)_{i=1..n} \rightarrow ((r_i)_{i=1..n-1}, d).$$

Conversely, the local sizes are calculated by:

$$h_i = d^{-\frac{1}{n}} r_i \text{ for } \; i = 1, .., n-1 \; \text{ and } \; h_n = d^{-\frac{1}{n}} \left(\prod_{i=1}^{n-1} r_i \right). \tag{13}$$

The intermediate pivot variable P is defined as $P = \left(\prod_{i=1}^{n-1} r_i \right)^{-1}$. Finally, after the substitution (13) we face the following problem to solve:

$$\min_{((r_i)_i, d)} \int_{\mathbf{x} \in \Omega} d^{-\frac{2p}{n}}(\mathbf{x}) \left(\sum_{i=1}^{n-1} r_i^2(\mathbf{x}) \left| \frac{\partial^2 u}{\partial {\alpha_i}^2}(\mathbf{x}) \right| + P^{-2}(\mathbf{x}) \left| \frac{\partial^2 u}{\partial {\alpha_n}^2}(\mathbf{x}) \right| \right)^p \mathrm{d}\mathbf{x}, \tag{14}$$

under the linear constraint:

$$\int_{\mathbf{x} \in \Omega} d(\mathbf{x}) \; \mathrm{d}\mathbf{x} = N. \tag{15}$$

4.2 Formal Resolution

In this section, we assume that the considered functions are smooth enough. The Euler-Lagrange optimality necessary condition reads: for a critical point $\mathcal{M}$, the variation of the cost function $\mathcal{E}$ is proportional to the variation of the constraint $\mathcal{C}$. Let $\delta\mathcal{E}(\mathcal{M}; \delta\mathcal{M})$ be the variation of the functional $\mathcal{E}$ in $\mathcal{M}$ in the direction $\delta\mathcal{M}$ defined as:

$$\delta\mathcal{E}(\mathcal{M}; \delta\mathcal{M}) = \lim_{\varepsilon \rightarrow 0} \frac{\mathcal{E}(\mathcal{M} + \varepsilon\, \delta\mathcal{M}) - \mathcal{E}(\mathcal{M})}{\varepsilon}.$$

As the number of vertices is constant, the variation of the constraint is zero:

$$\delta\mathcal{C}(\mathcal{M}; \delta\mathcal{M}) = \lim_{\varepsilon \rightarrow 0} \frac{1}{\varepsilon} \left(\int (d + \varepsilon d) - \int d \right) = \int \delta d = 0.$$

Then, we deduce by means of the Euler-Lagrange optimality necessary condition that it exists a Lagrange multiplier λ such that:

$$\forall \delta\mathcal{M}, \quad \delta\mathcal{E}(\mathcal{M}; \delta\mathcal{M}) = \lambda \delta C(\mathcal{M}; \delta\mathcal{M}) = 0\,,$$

or equivalently:

$$\forall \delta r_i \text{ for } i = 1, ..., n-1 \text{ and } \forall \delta d \text{ such that } \int \delta d = 0 \text{ then}$$

$$\sum_{i=1}^{n-1} \delta\mathcal{E}(\mathcal{M}; \delta r_i) + \delta\mathcal{E}(\mathcal{M}; \delta d) = 0\,, \tag{16}$$

where δr_i and δd are functions representing the different components of the variation $\delta\mathcal{M}$, i.e., $\delta\mathcal{M} = (\delta r_1, \delta r_2, .., \delta r_{n-1}, \delta d)$.

Problem (14)-(15) is solved in two distinct steps that are based on Equation (16):

- step 1: evaluation of the anisotropic quotients r_i for $i = 1, ..., n-1$
- step 2: evaluation of the density d, which is a normalization, to obtain the number of desired vertices N.

Step 1. If Equality (16) is developed by choosing $\delta d = 0$, it comes:

$$\int_\Omega 2^p d^{-\frac{2p}{n}} (*)^{p-1} \left(\sum_{i=1}^{n-1} \left(r_i \left| \frac{\partial^2 u}{\partial {\alpha_i}^2} \right| - P^{-2} r_i^{-1} \left| \frac{\partial^2 u}{\partial {\alpha_n}^2} \right| \right) \delta r_i \right) = 0, \tag{17}$$

where the term $(*)$ is equal to:

$$\sum_{i=1}^{n-1} r_i^2 \left| \frac{\partial^2 u}{\partial {\alpha_i}^2} \right| + P^{-2} \left| \frac{\partial^2 u}{\partial {\alpha_n}^2} \right| .$$

If the integrand of Equation (17) is zero then the equation is trivially satisfied and its solution is retained. It implies the $n-1$ following relations:

$$r_i \left| \frac{\partial^2 u}{\partial {\alpha_i}^2} \right| - P^{-2} r_i^{-1} \left| \frac{\partial^2 u}{\partial {\alpha_n}^2} \right| = 0 \text{ for } i = 1, ..., n-1 .$$

We deduce the $n-1$ first anisotropic quotients:

$$r_i = \left| \frac{\frac{\partial^2 u}{\partial {\alpha_n}^2}}{\frac{\partial^2 u}{\partial {\alpha_i}^2}} \right|^{\frac{1}{2}} P^{-1} \text{ for } i = 1, ..., n-1 . \tag{18}$$

Using the $n-1$ anisotropic quotients given by (18) and the fact that P is defined by the product of the inverse of the r_i for $i = 1, ..., n-1$, we have:

$$P = P^{-(n-1)} \left| \frac{\partial^2 u}{\partial {\alpha_n}^2} \right|^{\frac{n-1}{2}} \prod_{i=1}^{n-1} \left| \frac{\partial^2 u}{\partial {\alpha_i}^2} \right|^{-\frac{1}{2}} ,$$

then,

$$P = \left| \frac{\partial^2 u}{\partial {\alpha_n}^2} \right|^{\frac{1}{2}} \prod_{i=1}^{n} \left| \frac{\partial^2 u}{\partial {\alpha_i}^2} \right|^{-\frac{1}{2n}} . \tag{19}$$

From the previous relation, r_i for $i = 1, ..., n-1$ are exhibited independently of P:

$$r_i = \left| \frac{\partial^2 u}{\partial {\alpha_n}^2} \right|^{\frac{1}{2}} \left| \frac{\partial^2 u}{\partial {\alpha_i}^2} \right|^{-\frac{1}{2}} \left| \frac{\partial^2 u}{\partial {\alpha_n}^2} \right|^{-\frac{1}{2}} \prod_{i=1}^{n} \left| \frac{\partial^2 u}{\partial {\alpha_n}^2} \right|^{\frac{1}{2n}} ,$$

and finally,

$$r_i = \left| \frac{\partial^2 u}{\partial {\alpha_i}^2} \right|^{-\frac{1}{2}} \prod_{i=1}^{n} \left| \frac{\partial^2 u}{\partial {\alpha_i}^2} \right|^{\frac{1}{2n}}.$$

The anisotropic quotients may be also expressed in function of matrix $|H_u|$:

$$r_i = \left| \frac{\partial^2 u}{\partial {\alpha_i}^2} \right|^{-\frac{1}{2}} (\det |H_u|)^{\frac{1}{2n}} \text{ for } i = 1, ..., n-1\,.$$

Step 2. The evaluation of the density d is also deduced from Equality (17) by legally choosing $\delta r_i = 0$ for $i = 1, ..., n-1$, it results:

$$\int_\Omega d^{-\frac{2p+n}{n}} \left(\sum_{i=1}^{n-1} r_i^2 \left| \frac{\partial^2 u}{\partial {\alpha_i}^2} \right| + P^{-2} \left| \frac{\partial^2 u}{\partial {\alpha_n}^2} \right| \right)^p \delta d \; = 0. \tag{20}$$

A solution of the previous equality with δd verifying the constraint $\int \delta d = 0$ is obtained when the integrand that is multiplied by δd is constant. Therefore, we have:

$$d^{-\frac{2p+n}{n}} \left(\sum_{i=1}^{n-1} r_i^2 \left| \frac{\partial^2 u}{\partial {\alpha_i}^2} \right| + P^{-2} \left| \frac{\partial^2 u}{\partial {\alpha_n}^2} \right| \right)^p = Cst,$$

which, from Relations (18) and (19) equivalent to:

$$n^p d^{-\frac{2p+n}{n}} \left| \prod_{i=1}^{n} \frac{\partial^2 u}{\partial {\alpha_i}^2} \right|^{\frac{p}{n}} = Cst.$$

Finally, as the mesh must contain N vertices which are given by the integral of the density on Ω, the density reads:

$$d = N \left(\int_\Omega \left| \prod_{i=1}^{n} \frac{\partial^2 u}{\partial {\alpha_i}^2} \right|^{\frac{p}{2p+n}} \right)^{-1} \left| \prod_{i=1}^{n} \frac{\partial^2 u}{\partial {\alpha_i}^2} \right|^{\frac{p}{2p+n}}.$$

The density may also be written in function of the determinant of matrix $|H_u|$:

$$d = N \left(\int_\Omega (\det |H_u|)^{\frac{p}{2p+n}} \right)^{-1} (\det |H_u|)^{\frac{p}{2p+n}}.$$

Final solution. The solution of Problem (14)-(15) has been exhibited above. Then, the converse variables substitution given by Relation (13) is applied to solve Problem (11)-(12). For $i = 1, ..., n$, we have:

$$h_i = \frac{1}{N^{1/n}} \left(\int_\Omega (\det |H_u|)^{\frac{p}{2p+n}} \right)^{1/n} (\det |H_u|)^{\frac{1}{2(2p+n)}} \left| \frac{\partial^2 u}{\partial {\alpha_i}^2} \right|^{-1/2},$$

or equivalently,

$$\lambda_i = \frac{1}{h_i^2} = N^{2/n} \left(\int_\Omega (\det |H_u|)^{\frac{p}{2p+n}} \right)^{-2/n} (\det |H_u|)^{\frac{-1}{2p+n}} \left| \frac{\partial^2 u}{\partial {\alpha_i}^2} \right|.$$

4.3 Uniqueness and Order of Convergence

In this section, we will demonstrate by a direct proof that the obtained metric really minimize the error model. Let $\mathcal{M}$ be a metric define by $n-1$ anisotropic quotients r_i for $i = 1, ..., n-1$ and a density d which is written under the general form $d = N(\int_\Omega f)^{-1} f$. We recall that r_i for $i = 1, ..., n-1$ and f are strictly positive functions. From Relation (14), the error committed with this metric is given by:

$$\mathcal{E}(\mathcal{M}) = N^{-\frac{2p}{n}} \left(\int_\Omega f\right)^{-\frac{2p}{n}} \int_\Omega f^{-\frac{2p}{n}} \left(\sum_{i=1}^{n-1} r_i^2 \left|\frac{\partial^2 u}{\partial {\alpha_i}^2}\right| + \left|\frac{\partial^2 u}{\partial {\alpha_n}^2}\right| \prod_{i=1}^{n-1} r_i^{-2}\right)^p .$$

The error committed with the optimal metric $\mathcal{M}_{opt}$ is obtained with Relation (11):

$$\mathcal{E}(\mathcal{M}_{opt}) = n^p N^{-\frac{2p}{n}} \left(\int_\Omega \left|\prod_{i=1}^{n} \frac{\partial^2 u}{\partial {\alpha_i}^2}\right|^{\frac{p}{2p+n}}\right)^{\frac{2p+n}{n}} . \tag{21}$$

In order to prove that $\mathcal{E}(\mathcal{M}_{opt}) \leq \mathcal{E}(\mathcal{M})$, we use the generalized arithmetic-geometric inequality which comes from the concavity of ln:

$$\ln\left(\frac{1}{n}\sum_{i=1}^{n} r_i^2 \left|\frac{\partial^2 u}{\partial {\alpha_i}^2}\right|\right) \geq \frac{1}{n}\sum_{i=1}^{n} \ln\left(r_i^2 \left|\frac{\partial^2 u}{\partial {\alpha_i}^2}\right|\right) = \ln\left(\prod_{i=1}^{n} \left|\frac{\partial^2 u}{\partial {\alpha_i}^2}\right|^{\frac{1}{n}}\right) ,$$

as we have $\prod_{i=1}^{n} r_i = 1$. By substituting the value of r_n provided by Relation (13), it comes:

$$\sum_{i=1}^{n-1} ri^2 \left|\frac{\partial^2 u}{\partial {\alpha_i}^2}\right| + \left|\frac{\partial^2 u}{\partial {\alpha_n}^2}\right| \prod_{i=1}^{n-1} r_i^{-2} \;\geq\; n \left|\prod_{i=1}^{n} \frac{\partial^2 u}{\partial {\alpha_i}^2}\right|^{\frac{1}{n}} .$$

Finally, if we denote

$$g = \left|\prod_{i=1}^{n} \frac{\partial^2 u}{\partial {\alpha_i}^2}\right|^{\frac{p}{2p+n}} ,$$

we get

$$\begin{cases} \mathcal{E}(\mathcal{M}_{opt})^{\frac{n}{2p+n}} = n^{\frac{pn}{2p+n}} N^{-\frac{2p}{2p+n}} \displaystyle\int_\Omega g , \\ \mathcal{E}(\mathcal{M})^{\frac{n}{2p+n}} \quad \geq n^{\frac{pn}{2p+n}} N^{-\frac{2p}{2p+n}} \left(\displaystyle\int_\Omega f\right)^{\frac{2p}{2p+n}} \left(\displaystyle\int_\Omega f^{-\frac{2p}{n}} g^{\frac{2p++n}{n}}\right)^{\frac{n}{2p+n}} . \end{cases}$$

By utilizing the Holder inequality, we obtain

$$\left(\int_\Omega f^{\frac{2p}{2p+n}} \left(\frac{g}{f^{\frac{2p}{2p+n}}}\right)\right) \leq \left(\int_\Omega f\right)^{\frac{2p}{2p+n}} \left(\int_\Omega f^{-\frac{2p}{n}} g^{\frac{2p+n}{n}}\right)^{\frac{n}{2p+n}} , \tag{22}$$

as we have

$$\begin{cases} 1+\frac{n}{2p} \geq 1, \\ 1+\frac{2p}{n} \geq 1, \\ \frac{1}{1+\frac{n}{2p}} + \frac{1}{1+\frac{2p}{n}} = 1\,. \end{cases}$$

Therefore, Relation (22) implies that $\mathcal{E}(\mathcal{M}_{opt}) \leq \mathcal{E}(\mathcal{M})$, for all metric $\mathcal{M}$. As optimization Problem (14)-(15) is strictly convex, the solution is unique.

Order of Convergence

Let first introduce the definition of order of convergence in dimension n.

Definition. A sequence of n-d metrics $(\mathcal{M}_N)_N$ such that $\mathcal{C}(\mathcal{M}_N) = N$ vertices (cf. Relation (12)) gives a kth *order of convergence* for a given norm $\|e_{\mathcal{M}_N}(\mathbf{x})\|_{\mathbf{L}^p}$ if we have:

$$\|e_{\mathcal{M}_N}(\mathbf{x})\|_{\mathbf{L}^p} \leq Cst\ N^{-k/n}\,. \tag{23}$$

The pth square root of Relation (21) is considered to estimate the order of convergence:

$$\mathcal{E}^{1/p}(\mathcal{M}_{opt}) = nN^{-\frac{2}{n}} \left(\int_\Omega |\det(H_u)|^{\frac{p}{2p+n}} \right)^{\frac{2p+n}{pn}} \leq \frac{Cst}{N^{2/n}}.$$

Therefore, according to Relation (23), the previous inequality expresses a second-order of convergence of the metric sequence obtained by the present adaptation strategy for regular solutions whatever the chosen dimension and the chosen $\mathbf{L}^p$ norm.

5 Practical Continuous Metric in Three Dimensions

The metrics corresponding to the usual cases of the $\mathbf{L}^1$, $\mathbf{L}^2$ and $\mathbf{L}^\infty$ norms in three dimensions are presented. The $\mathbf{L}^\infty$ is found by passing to the limit. Notice that the obtained expression is exactly the same as the one based on geometric error estimate that has been commonly used in the literature [13].

The results are sum up with the following equation:

$$\mathcal{M}_{\mathbf{L}^p} = D_{\mathbf{L}^p}\, \mathcal{R}_u^{-1} \begin{pmatrix} \|\lambda_1\| & & \\ & \|\lambda_2\| & \\ & & \|\lambda_3\| \end{pmatrix} \mathcal{R}_u,$$

where $D_{\mathbf{L}^p}$ and λ_i for $i = 1, 2, 3$ are given in the following table:

Norm	$D_{\mathbf{L}^p}$	$\|\lambda_i\|$	Convergence order
$\mathbf{L}^p$	$N^{\frac{2}{3}}\left(\int_\Omega \left\|\prod_{i=1}^{3}\frac{\partial^2 u}{\partial {\alpha_i}^2}\right\|^{\frac{p}{2p+3}}\right)^{-\frac{2}{3}}$	$\left\|\frac{\partial^2 u}{\partial {\alpha_i}^2}\right\| \left\|\prod_{i=1}^{3}\frac{\partial^2 u}{\partial {\alpha_i}^2}\right\|^{-\frac{1}{2p+3}}$	2
$\mathbf{L}^1$	$N^{\frac{2}{3}}\left(\int_\Omega \left\|\prod_{i=1}^{3}\frac{\partial^2 u}{\partial {\alpha_i}^2}\right\|^{\frac{1}{5}}\right)^{-\frac{2}{3}}$	$\left\|\frac{\partial^2 u}{\partial {\alpha_i}^2}\right\| \left\|\prod_{i=1}^{3}\frac{\partial^2 u}{\partial {\alpha_i}^2}\right\|^{-\frac{1}{5}}$	2
$\mathbf{L}^2$	$N^{\frac{2}{3}}\left(\int_\Omega \left\|\prod_{i=1}^{3}\frac{\partial^2 u}{\partial {\alpha_i}^2}\right\|^{\frac{2}{7}}\right)^{-\frac{2}{3}}$	$\left\|\frac{\partial^2 u}{\partial {\alpha_i}^2}\right\| \left\|\prod_{i=1}^{3}\frac{\partial^2 u}{\partial {\alpha_i}^2}\right\|^{-\frac{1}{7}}$	2
$\mathbf{L}^\infty$	$N^{\frac{2}{3}}\left(\int_\Omega \left\|\prod_{i=1}^{3}\frac{\partial^2 u}{\partial {\alpha_i}^2}\right\|^{\frac{1}{2}}\right)^{-\frac{2}{3}}$	$\left\|\frac{\partial^2 u}{\partial {\alpha_i}^2}\right\|$	2

Notice that the metric could also be written:

$$\mathcal{M}_{\mathbf{L}^p} = D_{\mathbf{L}^p} \left(\det |H_u|\right)^{\frac{-1}{2p+3}} \mathcal{R}_u^{-1} \left|\Lambda\right| \mathcal{R}_u. \tag{24}$$

Relation (24) gives a quantitative physical interpretation of the impact of the norm on the metric construction. Indeed, the metric prescribes a fine size for a large eigenvalue of the Hessian. For the continuous metric, the eigenvalues are multiplied by the term $\left(\det |H_u|\right)^{\frac{-1}{2p+3}}$ which is small for large eigenvalues. Consequently, reducing p of the $\mathbf{L}^p$ norm implies to less refine large Hessian regions, for instance if a discontinuity occurs in the solution, it becomes less "attractive" for lower p. This will be illustrated in the next section on numerical examples.

6 Analytical Examples

In this section, we propose to analyze the impact of the continuous metric throughout a mesh adaptation process on two-dimensional and three-dimensional analytical examples. The mesh adaptation process is a single loop algorithm. We first apply the analytical function on the mesh, then the Hessian of the solution is computed by means of a double $\mathbf{L}^2$ projection algorithm. Finally, the continuous metric is constructed and a unit mesh with respect to this metric is generated. The process is repeated until convergence of the mesh. Notice that here the gradation of the mesh (the size variation between two neighboring elements) is not controlled.

As regards the mesh adaptation algorithm, the two-dimensional and three-dimensional methods are based on local mesh modifications. Each approach consists in modifying iteratively the initial mesh so as to complete a unit mesh

with respect to the metric $\mathcal{M}$. The ingredients to comply with these requirements typically include mesh enrichment, mesh coarsening and local mesh optimization procedures. The local mesh modification operators involved are: edge flipping, edge collapsing, edge splitting, node repositioning and degree relaxation.

The surface mesh modification algorithm, also used for the two-dimensional case, is pretty straightforward, edge lengths are computed with respect to the metric $\mathcal{M}$ and edges too small are collapsed while edges too long are splitted into unit length segments. Edge flips and node repositioning operations are performed to improve the overall size and shape mesh quality [11].

Similarly, in the volume mesh modification algorithm edge lengths are computed with respect to the metric $\mathcal{M}$ and edges too small are collapsed while edges too long are splitted using a vertex insertion procedure based on an anisotropic generalization of the Delaunay kernel [8]. Generalized edge swaps and node repositioning operations are performed to improve the overall size and shape mesh quality [15].

For each function, we compare meshes obtained for minimizing $\mathbf{L}^1$, $\mathbf{L}^2$ and $\mathbf{L}^\infty$ norms of the model error and we analyze the order of convergence obtained with each norm.

A Smooth Two-Dimensional Function

The first function f_1 is a smooth function involving small and large variation amplitudes, Figure 2 (top right). The function is defined as follow:

$$f_1(x,y) = \begin{cases} 0.1\,\sin(50\,x\,y) & \text{if} \quad x\,y \leq \dfrac{-\pi}{50} \\ \sin(50\,x\,y) & \text{if} \quad \dfrac{-\pi}{50} < x\,y \leq \dfrac{2\,\pi}{50} \\ 0.1\,\sin(50\,x\,y) & \text{if} \quad \dfrac{2\,\pi}{50} < x\,y \end{cases} \tag{25}$$

As we notice in Section 5, the metric defined with $\mathbf{L}^1$ norm better captures the small amplitudes than metrics constructed with norms with larger p. This is exemplified in Figure 2 where meshes are obtained for $\mathbf{L}^1$, $\mathbf{L}^2$ and $\mathbf{L}^\infty$ norms with a number of vertices targeted to $3,300$ are represented. Indeed, the small amplitude waves regions (in each corner) are more captured when using a $\mathbf{L}^p$ norm with a lower p whereas the large amplitude region is clearly more refined with the $\mathbf{L}^\infty$ norm.

In each case, the adapted mesh fits well the metric. The mesh adaptation algorithm statistics indicate that almost 91 % of the edges have a unit length, i.e., a length between $1/\sqrt{2}$ and $\sqrt{2}$. We can compute the efficiency index of the resulting adapted meshes, i.e., a scalar value representing the adequacy between the metric specification and the actual element size, with the following formula:

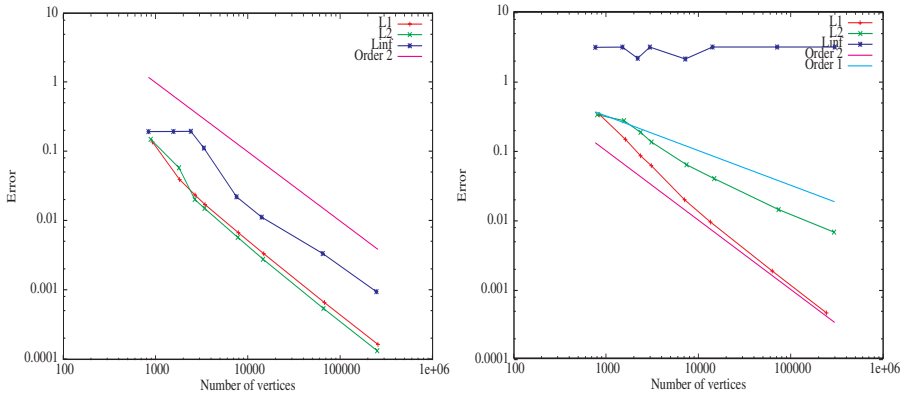

Fig. 1. Convergence order for functions f_1 (left) and f_2 (right) regarding the used $\mathbf{L}^p$ norm

$$\tau_{\mathcal{H}} = \exp\left(\frac{1}{n_e}\sum_{i=1}^{n_e}(Q_l(e_i)-1)\right),$$

where n_e is the number of edges of the mesh and $Q_l(e_i)$ is the length quality of the edge e_i in the metric given by:

$$Q_l(e_i) = \begin{cases} l_{\mathcal{M}}(e_i) & \text{if} \quad l_{\mathcal{M}}(e_i) \leq 1 \\ (l_{\mathcal{M}}(e_i))^{-1} & \text{else} \end{cases}$$

with $l_{\mathcal{M}}(e_i)$ the edge length in the metric $\mathcal{M}$. Here, an efficiency index close to 0.86 is obtained in each case.

Figure 3 shows the final mesh obtained for minimizing $\mathbf{L}^1$ norm of the error with a number of vertices targeted to $15,000$. The anisotropic mesh refinement along each wave is clearly emphasized in this figure.

For this function, a convergence of order 2 is reached for all norms as predicted by theory. This convergence is illustrated in Figure 1 (left).

A Steep-Gradient Two-Dimensional Function

The second analytic function f_2 is a function with small amplitude waves going through a sinusoidal steep-gradient step (similar to a Dirac layer) in the middle of the domain, Figure 4 (top right). The function is defined as follow:

$$f_2(x,y) = 0.1\,\sin(50\,x) + \arctan\left(\frac{0.1}{\sin(5\,y) - 2\,x}\right) \tag{26}$$

This function is proposed to point out the attractive effect of a steep-gradient region on the mesh adaptation process. As illustrated in Figure 4,

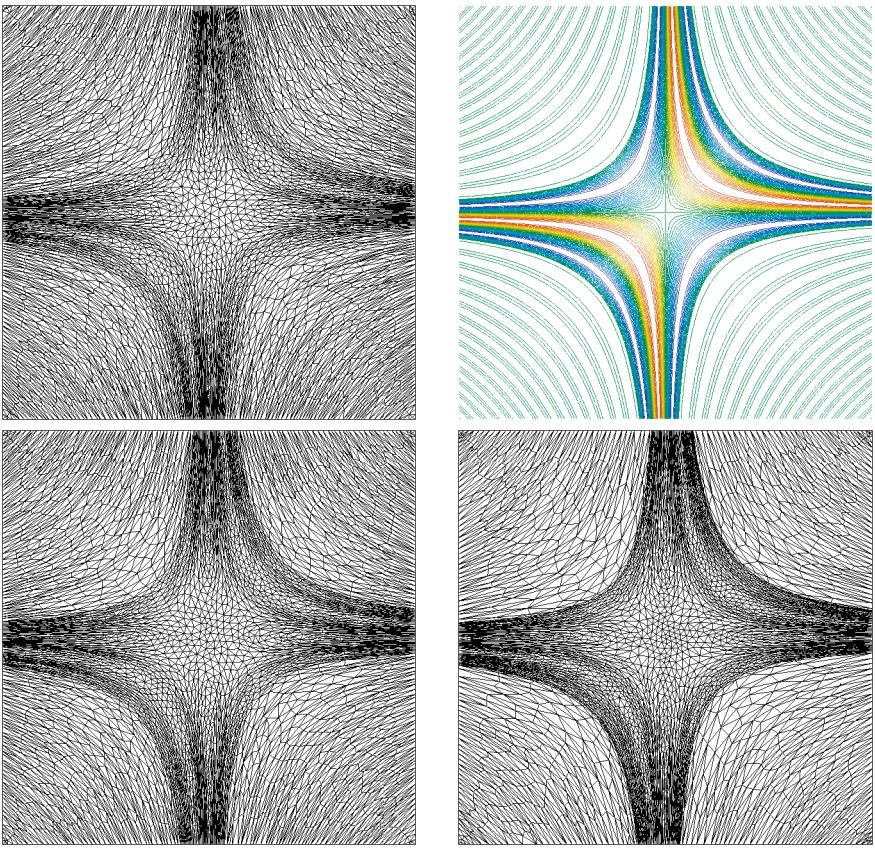

Fig. 2. Final adapted meshes minimizing $\mathbf{L}^1$ (top left), $\mathbf{L}^2$ (bottom left) and $\mathbf{L}^\infty$ (bottom right) norms with a target number of vertices equal to $3,300$ for the analytical function f_1. Top right, f_1 iso-values are represented

the mesh obtained ($N = 15,000$) with $\mathbf{L}^\infty$ norm only refines the steep-gradient region, whereas meshes with $\mathbf{L}^1$ and $\mathbf{L}^2$ norms were able to capture the small amplitude waves. Notice that even with $300,000$ vertices $\mathbf{L}^\infty$ norm continues to impose only vertex insertion in the steep-gradient region. This example puts in evidence that metrics defined by a $\mathbf{L}^p$ norm with a low p value are more appropriate to capture weak phenomena in simulations involving large amplitude phenomena such as shocks in CFD.

For this harder case, it is more difficult for the adaptive mesh generator to respect the metric field, even more without any mesh gradation, as most of the vertices are inserted in the steep-gradient region. The adapted mesh for the $\mathbf{L}^1$ norm fits well the metric, about 93 % of the edges having a length between $1/\sqrt{2}$ and $\sqrt{2}$ and the efficiency index being 0.866. Nevertheless, only 51 % of the edges have a length between $1/\sqrt{2}$ and $\sqrt{2}$ for the $\mathbf{L}^\infty$ case which

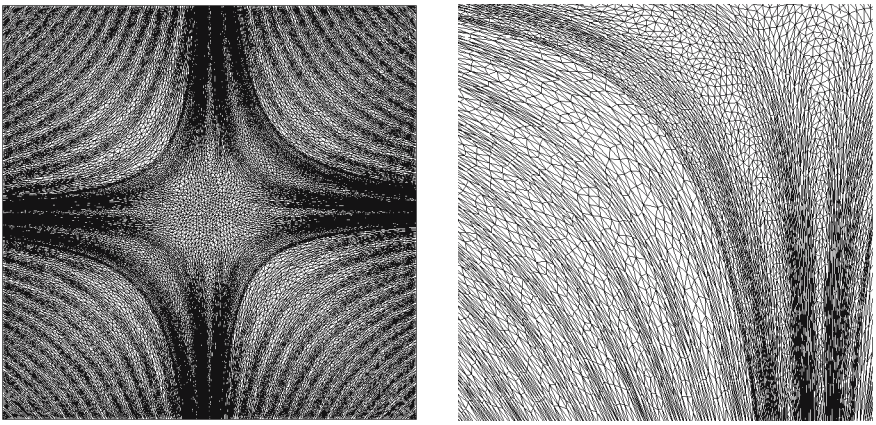

Fig. 3. Final adapted mesh minimizing $\mathbf{L}^1$ norm with a target number of vertices equal to $15,000$ for the analytical function f_1

leads to an efficiency index equal to 0.73 (notice that 80 % of the edges have a length between 1/2 and 2, mainly because of the lack of gradation control).

An order of convergence equal to 2 is only reached for $\mathbf{L}^1$ norm, whereas orders of 1 and 0 are obtained for $\mathbf{L}^2$ and $\mathbf{L}^\infty$ norms, respectively. Here, we don't want to drive any conclusion, as a complete analysis of the discontinuous cases must be assessed as in [6] where authors explained that theoretical orders of convergence are in some cases only asymptotically reached.

A Smooth Three-Dimensional Function

Function f_{3d} is a smooth function involving small and large variation amplitudes. f_{3d} is a three-dimensional extension of function f_1 in a spherical domain. The function is defined as follows:

$$f_{3d}(x,y,z) = \begin{cases} 0.1\,\sin(50\,\mathbf{x}) & \text{if } \mathbf{x} \leq \dfrac{-\pi}{50} \\ \sin(50\,\mathbf{x}) & \text{if } \dfrac{-\pi}{50} < \mathbf{x} \leq \dfrac{2\,\pi}{50} \\ 0.1\,\sin(50\,\mathbf{x}) & \text{if } \dfrac{2\,\pi}{50} < \mathbf{x} \end{cases} \tag{27}$$

where $\mathbf{x} = (x-0.4)\,(y-0.4)\,(z-0.4)$.

As mentioned previously in two dimensions, the metric defined with $\mathbf{L}^1$ norm better captures the small amplitudes than metrics constructed with norms with larger p. This is shown in Figures. 5 and 6 where anisotropic adapted surface and volume meshes are depicted for $\mathbf{L}^1$, $\mathbf{L}^2$ and $\mathbf{L}^\infty$ norms with a number of vertices targeted to $275,000$. The small variations of the function are clearly better captured with the $\mathbf{L}^1$ norm than the $\mathbf{L}^\infty$ norm.

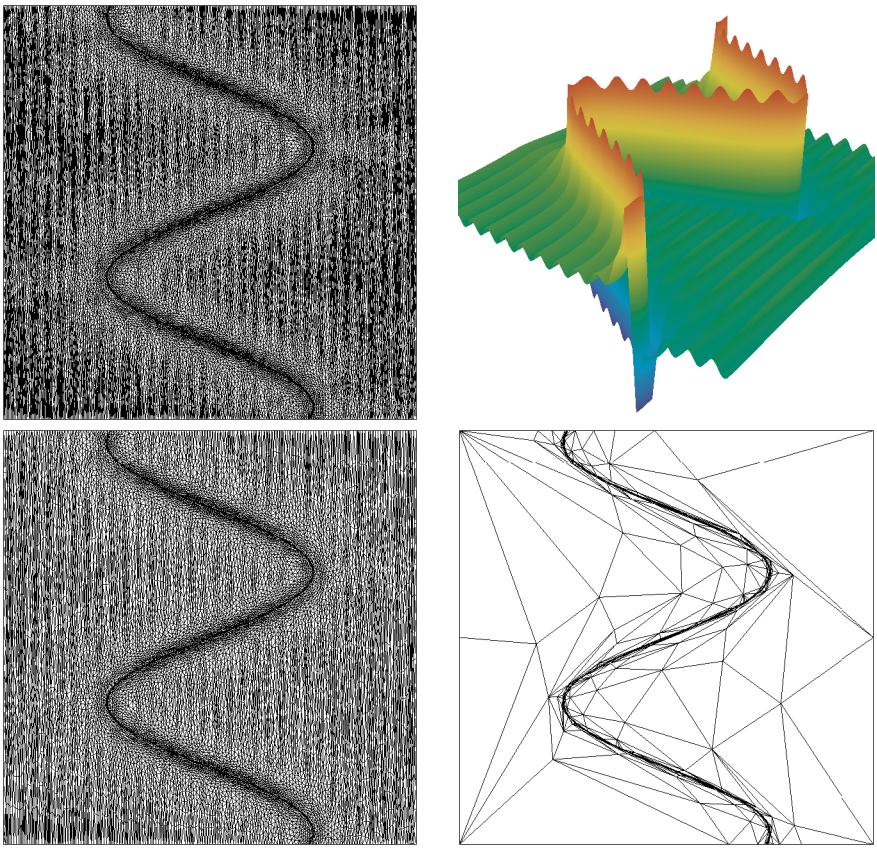

Fig. 4. Final adapted meshes minimizing $\mathbf{L}^1$ (top left), $\mathbf{L}^2$ (bottom left) and $\mathbf{L}^\infty$ (bottom right) norms with a target number of vertices equal to $15,000$ for the analytical function f_2. Top right, the surface described by f_2 is represented

In each case, the adapted tetrahedral mesh respects well the metric. Between 80 % and 85 % of the edges have a unit length and an efficiency index between 0.825 and 0.84 is obtained.

Order of convergence for this analytical function is presented in Figure 5 (top right). A convergence of order equal to 2 is reached for $\mathbf{L}^1$ and $\mathbf{L}^2$ norms as expected by theory. As for as $\mathbf{L}^\infty$ norm is concerned, second order convergence is not obtained regarding the global $\mathbf{L}^\infty$ norm over all the domain. Nevertheless, if the local $\mathbf{L}^\infty$ norm is integrated over the domain then an almost second order of convergence is observed. Indeed, this norm aims at equally distributing the interpolation error over the domain.

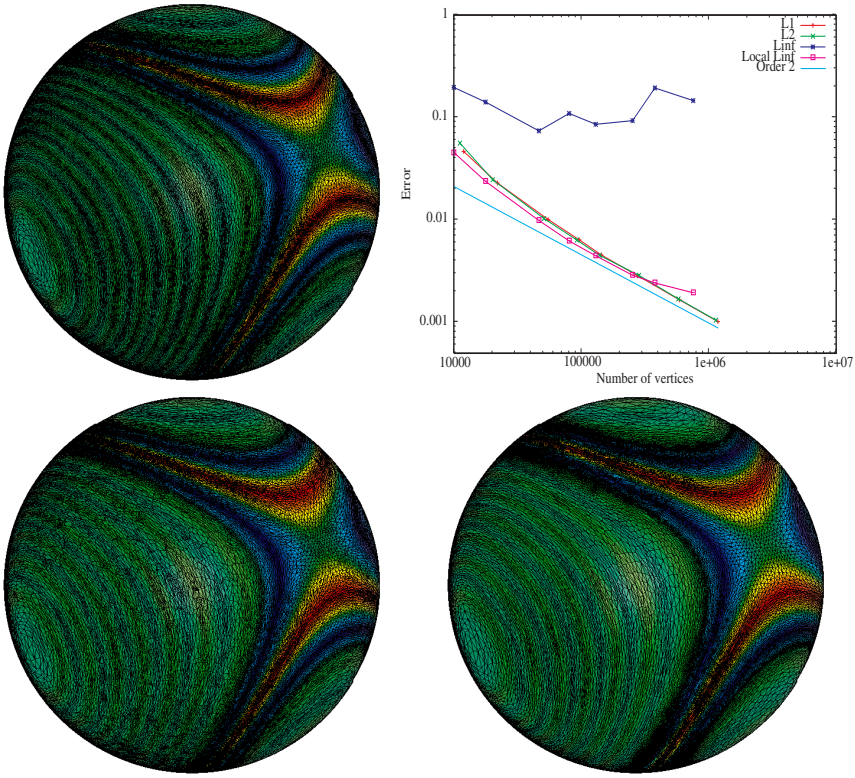

Fig. 5. Final anisotropic adapted surface meshes minimizing $\mathbf{L}^1$ (top left), $\mathbf{L}^2$ (bottom left) and $\mathbf{L}^\infty$ (bottom right) norms with a target number of vertices equal to $275,000$ for the analytical function f_{3d}. Top right, convergence order for function f_{3d} regarding the used $\mathbf{L}^p$ norm

7 Conclusion

In this paper, a continuous approach has been proposed to derive metrics in order to minimize the interpolation error in $\mathbf{L}^p$ norm. This approach is based on classes of equivalence between meshes represented by continuous metrics. We have demonstrated that there exists a unique optimal metric. A theoretical analysis gives the conditions for second-order convergence.

These theoretical results have been exemplified on analytical functions in two and three dimensions where second order of convergence have been observed.

In future work, we intend to apply this continuous setting to discontinuous solutions and to realistic three-dimensional numerical simulations.

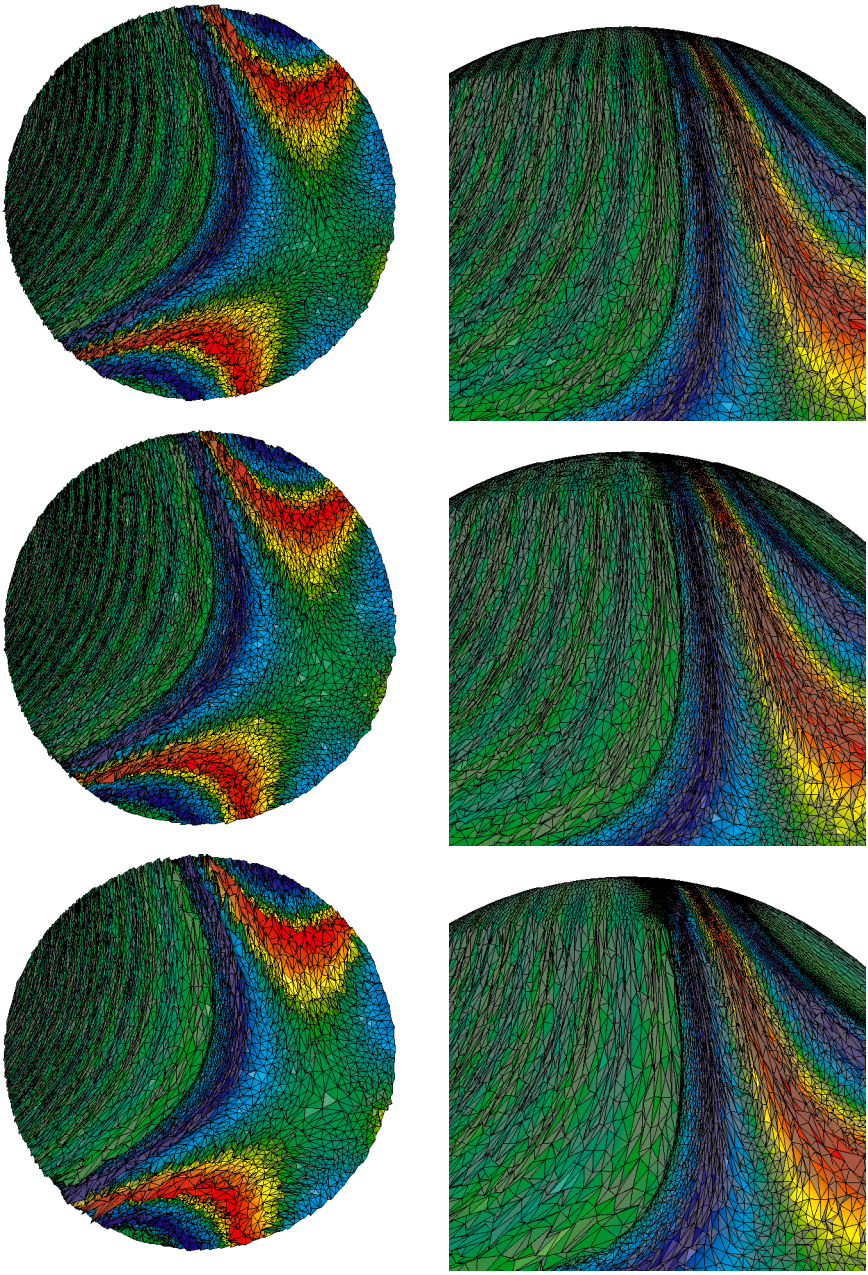

Fig. 6. Final anisotropic adapted volume meshes in a cut plane minimizing $\mathbf{L}^1$ (top), $\mathbf{L}^2$ (middle) and $\mathbf{L}^\infty$ (bottom) norms with a target number of vertices equal to $275,000$ for the analytical function f_{3d}

References

1. Almeida, R., Feijóo, R., Galeao, A., Padra, C., and Silva, R. Adaptive finite element computational fluid dynamics using an anisotropic error estimator. *Comput. Methods Appl. Mesh. Engrg. 182* (2000), 379–400.
2. Biswas, R., and Strawn, R. A new procedure for dynamic adaption of three-dimensional unstructured grids. *Applied Numerical Mathematics 13* (1994), 437–452.
3. Buscaglia, G., and Dari, E. Anisotropic mesh optimization and its application in adaptivity. *Int. J. Numer. Meth. Engng 40* (1997), 4119–4136.
4. Castro-Diaz, M., Hecht, F., Mohammadi, B., and Pironneau, O. Anisotropic unstructured mesh adaptation for flow simulations. *Int. J. Numer. Meth. Fluids 25* (1997), 475–491.
5. Chen, L., Sun, P., and Xu, J. Optimal anisotropic simplicial meshes for minimizing interpolation errors in L^p-norms. *Math. Comp. 0* (2006). to appear.
6. Courty, F., Leservoisier, D., George, P.-L., and Dervieux, A. Continuous metrics and mesh adaptation. *Applied Numerical Mathematics 56* (2006), 117–145.
7. Dervieux, A., Leservoisier, D., George, P.-L., and Coudiere, Y. About theoretical and practical impact of mesh adaptations on approximation of functions and of solution of pde. *Int. J. Numer. Meth. Fluids 43* (2003), 507–516.
8. Dobrzynski, C. *Adaptation de maillage anisotrope 3D et application à l'aérothermique des bâtiments.* PhD thesis, Université Pierre et Marie Curie, Paris VI, Paris, France, 2005. (in French).
9. Dompierre, J., Vallet, M., Fortin, M., Bourgault, Y., and Habashi, W. Anisotropic mesh adaptation: towards a solver and user independent cfd. *AIAA paper 97-0861* (1997).
10. Formaggia, L., Micheletti, S., and Perotto, S. Anisotropic mesh adaptation in computational fluid dynamics: Application to the advection-diffusion-reaction and the Stokes problem. *Applied Numerical Mathematics 51* (2004), 511–533.
11. Frey, P. About surface remeshing. In *Proc. of 9th Int. Meshing Rountable* (New Orleans, LO, USA, 2000), pp. 123–136.
12. Frey, P., and Alauzet, F. Anisotropic mesh adaptation for transient flows simulations. In *Proc. of 12th Int. Meshing Rountable* (Santa Fe, New Mexico, USA, 2003), pp. 335–348.
13. Frey, P., and Alauzet, F. Anisotropic mesh adaptation for CFD computations. *Comput. Methods Appl. Mech. Engrg. 194*, 48-49 (2005), 5068–5082.
14. Frey, P., and George, P.-L. *Mesh generation. Application to finite elements.* Hermès Science, Paris, Oxford, 2000.
15. George, P.-L., and Borouchaki, H. Back to edge flips in 3 dimensions. In *Proc. of 12th Int. Meshing Rountable* (Santa Fe, NM, USA, 2003), pp. 393–402.
16. Gruau, C., and Coupez, T. 3D tetrahedral, unstructured and anisotropic mesh generation with adaptation to natural and multidomain metric. *Comput. Methods Appl. Mech. Engrg. 194*, 48-49 (2005), 4951–4976.
17. Huang, W. Metric tensors for anisotropic mesh generation. *J. Comput. Phys. 204* (2005), 633–665.
18. Kallinderis, Y., and Vijayan, P. Adaptive refinement-coarsening scheme for three-dimensional unstructured meshes. *AIAA Journal 31*, 8 (1993), 1440–1447.

19. Leservoisier, D., George, P.-L., and Dervieux, A. Métrique continue et optimisation de maillage. RR-4172, INRIA, Apr. 2001. (in French).
20. Li, X., Shephard, M., and Beall, M. 3D anisotropic mesh adaptation by mesh modification. *Comput. Methods Appl. Mech. Engrg. 194*, 48-49 (2005), 4915–4950.
21. Löhner, R., and Baum, J. Adaptive h-refinement on 3D unstructured grids for transient problems. *Int. J. Numer. Meth. Fluids 14* (1992), 1407–1419.
22. Mavriplis, D. Adaptive meshing techniques for viscous flow calculations on mixed-element unstructured meshes. *AIAA paper 97-0857* (1997).
23. Pain, C., Humpleby, A., de Oliveira, C., and Goddard, A. Tetrahedral mesh optimisation and adaptivity for steady-state and transient finite element calculations. *Comput. Methods Appl. Mech. Engrg. 190* (2001), 3771–3796.
24. Peraire, J., Peiro, J., and Morgan, K. Adaptive remeshing for three-dimensional compressible flow computations. *J. Comput. Phys. 103* (1992), 269–285.
25. Rausch, R., Batina, J., and Yang, H. Spatial adaptation procedures on tetrahedral meshes for unsteady aerodynamic flow calculations. *AIAA Journal 30* (1992), 1243–1251.
26. Schall, E., Leservoisier, D., Dervieux, A., and Koobus, B. Mesh adaptation as a tool for certified computational aerodynamics. *Int. J. Numer. Meth. Fluids 45* (2004), 179–196.
27. Speares, W., and Berzins, M. A 3d unstructured mesh adaptation algorithm for time-dependent shock-dominated problems. *Int. J. Numer. Meth. Fluids 25* (1997), 81–104.
28. Tam, A., Ait-Ali-Yahia, D., Robichaud, M., Moore, M., Kozel, V., and Habashi, W. Anisotropic mesh adaptation for 3d flows on structured and unstructured grids. *Comput. Methods Appl. Mech. Engrg. 189* (2000), 1205–1230.